Chem Biol Drug Des 2012; **79:** 663–673

Research Article

© 2012 John Wiley & Sons A/S

doi: 10.1111/j.1747-0285.2012.01349.x

3′-Axial CH_2OH Substitution on Glucopyranose does not Increase Glycogen Phosphorylase Inhibitory Potency. QM/MM-PBSA Calculations Suggest Why

Stella Manta[1], Andromachi Xipnitou[1], Christos Kiritsis[1], Anastassia L. Kantsadi[1], Joseph M. Hayes[2,*], Vicky T. Skamnaki[2], Christos Lamprakis[2], Maria Kontou[1], Panagiotis Zoumpoulakis[2], Spyridon E. Zographos[2], Demetres D. Leonidas[1,*] and Dimitri Komiotis[1,*]

[1]Department of Biochemistry and Biotechnology, University of Thessaly, 26 Ploutonos Str., 41221 Larissa, Greece
[2]Institute of Organic and Pharmaceutical Chemistry, National Hellenic Research Foundation, 48 Vassileos Constantinou Avenue, 11635 Athens, Greece
**Corresponding author: Dimitri Komiotis, dkom@bio.uth.gr; Demetres D. Leonidas, ddleonidas@bio.uth.gr; Joseph M. Hayes, jhayes@eie.gr*

Glycogen phosphorylase is a molecular target for the design of potential hypoglycemic agents. Structure-based design pinpointed that the 3′-position of glucopyranose equipped with a suitable group has the potential to form interactions with enzyme's cofactor, pyridoxal 5′-phosphate (PLP), thus enhancing the inhibitory potency. Hence, we have investigated the binding of two ligands, 1-(β-D-glucopyranosyl)5-fluorouracil (GlcFU) and its 3′-CH_2OH glucopyranose derivative. Both ligands were found to be low micromolar inhibitors with K_i values of 7.9 and 27.1 μM, respectively. X-ray crystallography revealed that the 3′-CH_2OH glucopyranose substituent is indeed involved in additional molecular interactions with the PLP γ-phosphate compared with GlcFU. However, it is 3.4 times less potent. To elucidate this discovery, docking followed by postdocking Quantum Mechanics/Molecular Mechanics – Poisson–Boltzmann Surface Area (QM/MM-PBSA) binding affinity calculations were performed. While the docking predictions failed to reflect the kinetic results, the QM/MM-PBSA revealed that the desolvation energy cost for binding of the 3′-CH_2OH-substituted glucopyranose derivative out-weigh the enthalpy gains from the extra contacts formed. The benefits of performing postdocking calculations employing a more accurate solvation model and the QM/MM-PBSA methodology in lead optimization are therefore highlighted, specifically when the role of a highly polar/charged binding interface is significant.

Keywords: branched *C*-hydroxymethyl nucleosides, enzyme inhibition, glide docking, glycogen phosphorylase, QM/MM-PBSA, solvation modeling, type 2 diabetes, X-ray crystallography

Abbreviations: GlcFU, 1-(β-D-glucopyranosyl)5-fluorouracil; HMDS, hexamethyldisilazane; EtOAc, ethyl acetate; Ac_2O, acetic anhydride; MeOH, methanol; TMSOTf, trimethylsilyl trifluoromethanesulfonate; GP, glycogen phosphorylase; GPb, rabbit muscle glycogen phosphorylase b; PLP, pyridoxal 5′-phosphate; Glc-1-P, α-D-glucose 1-phosphate; rmsd, root-mean-square deviation; QM/MM-PBSA, Quantum Mechanics/Molecular Mechanics – Poisson–Boltzmann Surface Area; BFE, binding free energy.

Received 30 September 2011, revised 10 January 2012 and accepted 10 January 2012

Glycogen phosphorylase (GP) is a key enzyme in glycogen metabolism that catalyzes the first step in the intracellular degradation of glycogen (1). A large number of compounds have been reported to bind at five distinct binding sites (1–3): the catalytic, the allosteric, the new allosteric, the inhibitor and the glycogen storage site. The efficacy of such inhibitors on blood glucose control and hepatic glycogen balance has been confirmed from animal studies and *in vitro* cell biology experiments (4–8) validating GP as an important target for structure-based inhibitor design of new hypoglycemic agents for the treatment of diabetes type 2. Furthermore, the number of patents filed by pharmaceutical and biotechnology companies targeting GP for the discovery of novel hypoglycemic agents has been steadily increasing in the last 3 years (9).

Recently, we have investigated the binding of a series of 3′-fluorinated pyrimidine glucopyranonucleosides to GP which proved to be medium potency inhibitors with IC_{50} values ranging between 6.5 mM and 46.4 μM (10). All the 3′-glucose substituents were in the 3′-equatorial position. The 3′ carbon of glucose is 5 Å away from the γ-phosphate of pyridoxal 5′-phosphate (PLP) in the GPb-α-D-glucose complex (11), in the direction of the 3′-axial position. Suitable substituents at the 3′-axial position have therefore the potential to form interactions with the proximal PLP γ-phosphate (a mono-anion). Thus, building on our previous studies of modified nucleosides (10), we report here the synthesis, biochemical evaluation and the structural mode of binding to GPb of 1-[3′-*C*-(hydroxymethyl)-β-D-glucopyranosyl]5-fluorouracil (**5**) together with that of the parental

Table 1: The chemical structures of the inhibitors studied. The numbering scheme used is shown together with the K_i values for each inhibitor

Compound	Chemical structure	K_i (μM)
GlcFU	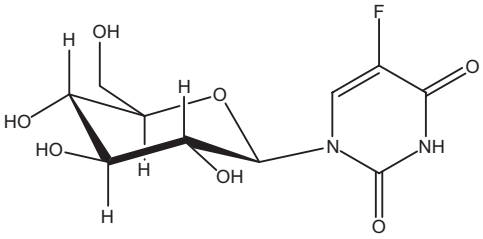	7.9 ± 0.3
5	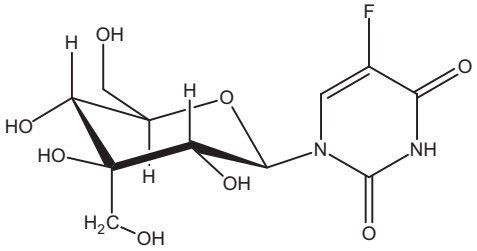	27.1 ± 1.4
	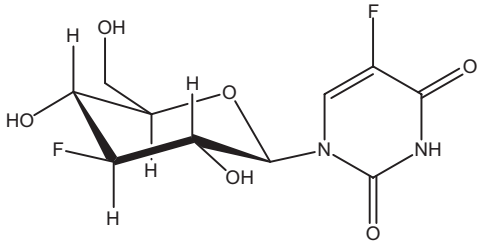	3670[a]

[a]Related 1-(3′-deoxy-3′-fluoro-β-D-glucopyranosyl)5-fluorouracil ligand with a 3′-equatorial substitution, as reported in our previous study (10).

compound 1-(β-D-glucopyranosyl)5-fluorouracil (GlcFU) for comparison reasons, given that its structural mode of binding has not yet been reported. The ligand structures are displayed in Table 1.

Molecular modeling calculations are now frequently applied in GP inhibitor design (12). Here, Glide-XP (13) docking calculations followed by Quantum Mechanics/Molecular Mechanics – Poisson–Boltzmann Surface Area (QM/MM-PBSA) binding free energy (BFE) calculations were employed to further analyze and explain our kinetics results.

Materials and Methods

Organic synthesis

General methods

Melting points were recorded on a Mel-Temp apparatus and are uncorrected. Thin layer chromatography (TLC) was performed on Merck precoated $60F_{254}$ plates. Reactions were monitored by TLC on silica gel, with detection by UV light (254 nm) or by charring with sulfuric acid. Flash column chromatography was performed using silica gel (240–400 mesh; Merck Chemicals, Frankfurt, Germany). ^{1}H, ^{19}F, and ^{13}C NMR spectra were obtained at room temperature with a Bruker 400 spectrometer at 400, 376, and 100 MHz, respectively, using $CDCl_3$ and methanol-d_4 (CD_3OD) with internal tetramethylsilane (TMS) for ^{1}H and ^{13}C and internal trifluorotoluene for ^{19}F. Chemical shifts (δ) were given in ppm measured downfield from TMS, and spin–spin coupling constants are in Hz. UV–Vis spectra were recorded on a PG T70 UV–VIS spectrometer, and mass spectra were obtained with a Micromass Platform LC (ESI-MS). Optical rotations were measured using an Autopol I polarimeter. Acetonitrile was distilled from calcium hydride and stored over 3E molecular sieves.

3-*C*-Acetoxymethyl-1,2,4,6-tetra-*O*-acetyl-D-glucopyranose 3

To a solution of **2** (14,15) (2.65 g, 7.96 mmol) in MeOH (12.4 mL) and H_2O (71.1 mL), Amberlite IR 120 (H^+) resin was added and the mixture was refluxed overnight, filtered, and evaporated to dryness. The residual gum was then dissolved in a mixture of pyridine (20.2 mL) and Ac_2O (10.6 mL) and the resulted mixture stirred at room temperature for 1 h. MeOH (0.40 mL) was added at 0 °C and the mixture was concentrated under high vacuum to remove the solvents. The residue was diluted with EtOAc and washed with saturated sodium bisulfate, sodium bicarbonate and water. The organic extracts were dried over anhydrous sodium sulfate, filtered, and evaporated to dryness to give anomeric acetates **3** (1.81 g, 54%, R_f = 0.28 in hexane/EtOAc, 1:1) as a yellow foam. $[\alpha]_D^{22}$ + 13.0 (*c* 0.50, $CHCl_3$); ^{1}H NMR ($CDCl_3$): δ 6.45 and 6.04 (α: d, $J_{1',2'}$ = 4.3 Hz, 0.43H, H-1; β: d, $J_{1',2'}$ = 9.7 Hz, 0.57H, H-1), 5.41–5.08 (m, 3H), 4.63–4.19 (m, 3H), 3.48–3.35 (m, 2H), 2.14–2.06 (m, 15H, OAc). Anal. Calcd for $C_{17}H_{24}O_{12}$: C, 48.57; H, 5.75. Found: C, 48.45; H, 5.98. ESI-MS (*m/z*): 421.4 ($M+H^+$).

1-[2′,4′,6′-Tri-*O*-acetyl-3′-*C*-(acetoxymethyl)-β-D-glucopyranosyl]5-fluorouracil 4

A mixture of 5-fluorouracil (0.78 g, 6.02 mmol), hexamethyldisilazane (HMDS) (1.57 mL, 7.46 mmol), and saccharin (0.051 g, 0.28 mmol) in dry CH_3CN (21 mL) was refluxed for 30 min. 3-*C*-Acetoxymethyl-1,2,4,6-tetra-*O*-acetyl-D-glucopyranose (**3**) (1.81 g, 4.30 mmol) and trimethylsilyl trifluoromethanesulfonate (TMSOTf) (1.09 mL, 6.02 mmol) were added and the reaction mixture was refluxed for 1.5 h, neutralized with saturated sodium bicarbonate, and then extracted with CH_2Cl_2. The organic extracts were dried over anhydrous sodium sulfate, filtered, and evaporated to dryness. The residue was purified by flash chromatography (hexane/EtOAc, 4:6) to give compound **4** (1.27 g, 60%, R_f = 0.32 in hexane/EtOAc, 4:6) as a white foam. $[\alpha]_D^{22}$ - 2.0 (*c* 0.11, $CHCl_3$); λ_{max} ($CHCl_3$) 265 nm (ε 4608). ^{1}H NMR ($CDCl_3$): δ 8.80 (br s, 1H, NH), 7.54 (d, 1H, $J_{F5,6}$ = 5.9 Hz, H-6), 6.25 (dd, 1H, $J_{1',2'}$ = 9.6 Hz, $J_{1',F5}$ = 1.6 Hz, H-1′), 5.20 (d, 1H, $J_{2',1'}$ = 9.6 Hz, H-2′), 5.13 (d, 1H, $J_{4',5'}$ = 9.8 Hz, H-4′), 4.47 (d, 1H, $J_{a,b}$ = 11.8 Hz, H-3a′′), 4.33–4.26 (m, 3H, H-5′, H-6a′, H-6b′), 4.19 (d, 1H, $J_{a,b}$ = 11.8 Hz, H-3b′′), 3.72 (br s, 1H, OH), 2.22, 2.20, 2.13, 2.10 (4s, 12H, 4OAc). ^{19}F NMR: δ –65.0; Anal. Calcd for $C_{19}H_{23}FN_2O_{12}$: C, 46.54; H, 4.73; N, 5.71. Found: C, 46.42; H, 4.82; N, 6.03. ESI-MS (*m/z*): 491.4 ($M+H^+$).

1-[3′-*C*-(Hydroxymethyl)-β-D-glucopyranosyl]5-fluorouracil 5

Compound **4** (1.27 g, 2.58 mmol) was treated with ammonia/MeOH (saturated at 0 °C, 106 mL). The solution was stirred overnight at room temperature and then was concentrated under reduced pressure to give compound **5** (0.75 g, 90%, R_f = 0.2 in EtOAc/MeOH, 9:1) as a white foam. $[\alpha]_D^{22}$ + 2.0 (*c* 0.17, MeOH); λ_{max} (MeOH) 266 nm (ε 1910); ^{1}H NMR (CD_3OD): δ 7.94 (d, 1H, $J_{F5,6}$ = 6.7 Hz, H-6), 6.01 (dd, 1H, $J_{1',2'}$ = 9.6 Hz, $J_{1',F5}$ = 1.7 Hz, H-1′), 3.91–3.88 (m, 1H, H-5′), 3.82 (dd, 2H, $J_{a,b}$ = 12.1 Hz, H-3′′), 3.74–3.66 (m, 2H, H-2′, H-4′), 3.63–3.69 (m, 2H, H-6a′, H-6b′).^{13}C NMR (CD_3OD): δ 158.30, 150.89, 140.23, 128.35, 82.15, 76.56, 75.57, 71.03, 62.52, 61.69, 58.05. ^{19}F NMR: δ –64.3; Anal. Calcd for $C_{11}H_{15}FN_2O_8$: C, 41.00; H, 4.69; N, 8.69. Found: C, 40.74; H, 4.82; N, 8.85. ESI-MS (*m/z*): 323.3 ($M+H^+$).

Enzyme isolation and kinetic experiments

Glycogen phosphorylase (GPb) was isolated from rabbit skeletal muscle and purified as described previously (16). Kinetic studies were performed in the direction of glycogen synthesis with 5 μg/mL enzyme, constant concentrations of glycogen (0.2% w/v), AMP (1 mM), and Glc-1-P (2, 4, 6, 10 and 20 mM) and various concentrations of inhibitors in a buffer of 30 mM imidazole/HCl (pH 6.8) containing 60 mM KCl, 0.6 mM EDTA, and 0.6 mM dithiothreitol. Enzyme activity was measured at pH 6.8 by the release of inorganic phosphate as previously described (10).

X-ray crystallography

GPb crystals, grown in the tetragonal lattice, space group $P4_32_12$, as previously described(10) were soaked with 2 mM of GlcFU, or of **5** in a solution of the crystallization media 2.0 h prior to data collection. Diffraction data were collected using a hi-flux Cu X-ray microfocus source (Oxford Diffraction SuperNova Oxford, U.K.) equipped with a 4 kappa goniometer and the ATLAS CCD (135 mm) detector at room temperature. Crystal orientation, integration of reflections, inter-frame scaling, and partial reflection summation were performed by the program Crysalis (17). Data reduction and integration followed by scaling and merging of the intensities obtained were performed with the program SCALA of the CCP4 suite of programs (18). Crystallographic refinement of the complexes was performed by maximum-likelihood methods using REFMAC (18). The starting model employed for the refinement of the complexes was the structure of the native T state GPb complex determined at 1.9 Å resolution (Leonidas, D.D., Skamnaki, V.T., Zographos, S.E., Johnson, L.N., and Oikonomakos, N.G. *et al.*, unpublished results). Ligand models were constructed using the PRODRG server (19) and they were fitted to the electron density maps after adjustment of their torsion angles. Alternate cycles of manual rebuilding with the molecular graphics program COOT (20) and refinement with REFMAC (21) improved the quality of the models. The stereochemistry of the protein residues was validated by MolProbity (22). Hydrogen bonds and van der Waals interactions were calculated with the program CONTACT as implemented in CCP4 (18) applying a distance cut-off of 3.3 and 4.0 Å, respectively. Protein structures were superimposed using LSQKAB as implemented in CCP4 (18). Figures were prepared with the programs MOLSCRIPT (23) and PYMOL (24). The coordinates of the new structures have been deposited with the RCSB Protein Data Bank (http://www.rcsb.org/pdb) with codes presented in Table 1.

Computational details

Protein preparation

The initial setup of the GPb receptor for calculations was performed using Schrodingers' 'Protein Preparation Wizard' (13) starting from the GPb-**5** complex. Water molecules within 5 Å of the ligand were retained for the protein preparation to account for their influence on the hydrogen bonding network, but deleted for the subsequent docking and QM/MM-PBSA calculations. Bond orders were assigned and hydrogen atoms added, with protonation states for basic and acidic residues based on residue pKa's at normal pH (7.0). However, subsequent optimization of hydroxyl, histidine protonation states and C/N atom 'flips', and side chain O/N atom 'flips' of Asn and Gln was based on optimizing hydrogen bonding patterns, so that the final assignments were checked on visual inspection of the protein. In particular, all final His residues were assigned as neutral, either in a HIE (hydrogen on epsilon nitrogen) or in a HID (hydrogen on delta nitrogen) state. Notably, the His377 was used in a HID state which we have previously validated (10) using PDB2PQR (25) and PROPKA (26) calculations. The γ-phosphate in PLP was assigned mono-anion form. Finally, an 'Impref' minimization of the GPb complex was performed using the OPLS-AA (2005) force field to remove steric clashes and bad contacts. At the end of the minimization, the RMSD of all heavy atoms was within 0.3 Å of the crystallographic positions.

Ligand preparation

The ligands GlcFU and **5** were extracted from their respective crystal structure complexes and prepared for calculations using Maestro and LigPrep (13).

Docking Calculations

Flexible ligand docking calculations of GlcFU and **5** to the 'prepared' GPb structure were performed using the program Glide version 5.0(13). The shape and properties of the GPb catalytic binding-site were first mapped onto grids with dimensions of ~21.8 Å × 21.8 Å × 21.8 Å centered on the native ligand. Docking calculations were performed in extra-precision (XP) mode with standard van der Waals scaling (by 0.8) of non-polar ligand atoms. Core constraints on the six glucose ring atoms were used together with positional constraints on the hydroxyl oxygens of glucose and carbonyl oxygen of the uracil moiety. Such constraints were applied given their effectiveness for improving accuracy in previous work (10,12,27). Postdocking minimization of the ligand poses was performed with the poses considered conformationally distinct if their RMSD (heavy atoms) was larger than 0.5 Å.

QM/MM-PBSA calculations

Ligand BFEs were calculated using the QM/MM-PBSA method. QM/MM-PBSA is based on the traditional MM-PB(GB)SA approach (28) where the free energy of each state (receptor, ligand and complex) is estimated using eqn 1.

$$G = \langle E_{MM} \rangle + \langle G_{solv} \rangle - T\langle S_{MM} \rangle \quad (1)$$

E_{MM} and S_{MM} represent the total molecular mechanics (internal, electrostatic, and van der Waals) energy and an entropy estimate, respectively; G_{solv}, the solvation free energy. The terms in eqn 1 are normally averages obtained over molecular dynamics (MD) trajectories, although recently the effectiveness of alternatively using selected or single binding conformations (which is less computationally demanding) has been highlighted (29–32). It is hoped, therefore, that use of QM/MM-PBSA as a postdocking method may show similar success; it should be noted also in this regard that use of experimental type geometries (as determined by our RMSDs to the crystallographic ligand binding conformations) further increases the probability for successful predictions. So, in the QM/MM-PBSA approach used here, the (single) docking poses rather than MD snapshots are used, and the E_{MM} term is effectively replaced by the gas phase QM/MM energy:

$$G = E_{QM/MM} + G_{solv} - TS_{MM} \quad (2)$$

Binding free energies were then estimated as the difference in energies between the bound and unbound states of the protein–ligand complexes using eqn 3:

$$\Delta G_{bind} = \Delta E_{QM/MM} + \Delta G_{solv} - T\Delta S_{MM} \quad (3)$$

DFT with the B3LYP functional (33) and 6–31 + G* basis set (34) was used for the QM region, the ligands, while the GPb protein was described using MM with the OPLS-AA(2005) force field and without employing a non-bonded cut-off. The default solute (internal) dielectric constant of 1.0 was used. The MM region polarizes the QM region, where interactions between the QM and MM regions include electrostatic effects between the MM point charges and the QM wavefunction, and van der Waals terms between QM and MM atoms (35). Bulk solvation effects were accounted for using PBSA (36). Solving the Poisson–Boltzmann (PB) equation exploiting the quantum mechanics charge density for the QM region should in theory lead to more accurate predictions. The ΔG_{solv} term can be further decomposed:

$$\Delta G_{solv} = \Delta G_{PB}^{solv} + \Delta G_{SA}^{solv} \quad (4)$$

where ΔG_{PB}^{solv} accounts for the polar contributions, and ΔG_{SA}^{solv} the non-polar contributions proportional to changes in the solvent accessible surface areas. The latter term includes the cost of forming a cavity in solution, the attractive dispersion and solvent-structure perturbation (37). Hence, the entropy change of the solvent on ligand binding is included in the ΔG_{SA}^{solv} term, although part of the entropy is also hidden in the ΔG_{PB}^{solv} term via the temperature dependence of the dielectric constant (38). ΔG_{PB}^{solv}, however, is predominantly (electrostatic) solvation enthalpy effects. Meanwhile, the solute entropy contribution, ΔS_{MM} in eqn 3, was calculated using Rigid Rotor Harmonic Oscillator calculations (default options) with MacroModel 9.9 (13) and the OPLS-AA(2005) forcefield; using this algorithm, the change in vibrational, rotational and translational entropy of the ligands on binding was estimated and included.

For the QM/MM-PBSA calculations, the Glide-XP docking poses were used directly but also, for comparison, the relaxed poses following QM/MM gas phase optimizations. In the optimizations, the ligands (QM region) were free but the GPb receptor (MM region) held rigid (frozen). However, we also probed the effect of including a small flexible region in the protein, residues within 4 Å of the ligands allowed to be free in the optimizations. As before, B3LYP/6-31 + G* (33) and OPLS-AA(2005) were used for QM and MM regions, respectively. All QM/MM and QM/MM-PBSA calculations were performed using QSITE 5.7. (13)

Results and Discussion

Organic Synthesis

The synthesis of GlcFU has been described previously (39). Our synthetic strategy to the target 3′-*C*-hydroxymethyl nucleoside analogue was first to synthesize the suitable glycosyl donor as the key intermediate and then to carry out a condensation reaction with the nucleosidic base. Synthesis of the glycosyl donor 3-*C*-acetoxymethyl-1,2,4,6-tetra-*O*-acetyl-D-glucopyranose (**3**) is depicted in Scheme 1.

1,2:5,6-Di-*O*-isopropylidene-3-deoxy-3-methylene-D-glucofuranose (**1**) (40) was converted to the monoacetyl ether **2** by stereoselective *cis*-dihydroxylation using catalytic amount of osmium (VIII) oxide and *N*-methyl morpholine-*N*-oxide (14) and subsequent acetylation of the primary hydroxyl group of resulting diol (15). Hydrolysis of 3-*C*-branched derivative **2** using Amberlite IR 120 (H^+) resin in MeOH followed by subsequent treatment with Ac_2O in pyridine afforded a mixture of the anomeric acetates **3** (ratio of α to β anomer, 0.43:0.57). Condensation of the anomeric mixture **3** with per-*O*-silylated 5-fluorouracil using trimethylsilyl trifluoromethanesulfonate (TMSOTf) as the catalyst in acetonitrile (41) gave exclusively, due to the participation of 2′-acetoxy group, the protected β-nucleoside analogue **4**, in 60% yield. Finally, removal of all *O*-acetyl protecting groups of **4** with saturated methanolic ammonia afforded the target

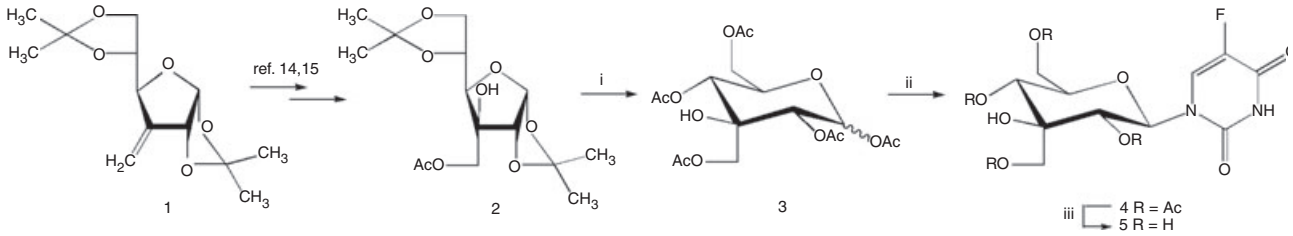

Scheme 1: (i) (A) H_2O, MeOH, Amberlite IR 120(H^+); (B) Ac_2O, pyridine; (ii) silylated 5-fluorouracil, TMSOTf, dry CH_3CN; (iii) ammonia/MeOH.

1-[3′-*C*-(hydroxymethyl)-β-D-glucopyranosyl]5-fluorouracil (**5**), in quantitative yield (90%).

All new compounds were well-characterized by NMR and UV spectroscopy, mass spectrometry, and elemental analysis. The structure elucidation of the newly synthesized 1-[2′,4′,6′-tri-*O*-acetyl-3′-*C*-(acetoxymethyl)-β-D-glucopyranosyl]5-fluorouracil (**4**), was made on the basis of its spectroscopic data. Therefore, in the ^{1}H NMR spectrum of **4**, proton H-1′ shows a large coupling with H-2′ ($J_{1',2'}$ = 9.6 Hz) indicating an axial orientation of both protons and thus an equatorially oriented 5-fluorouracil ring, as it was expected. The proposed structure for the novel 3′-*C*-branched nucleoside was further supported by NOE measurements performed on compound **4** as depicted in Figure S1 in the supplementary section. The mutual NOE enhancements observed between axial H-1′ with both H-3a″ and H-3b″ of the acetoxymethyl moiety show that these protons are at the same side of the plane. Similarly, the significant mutual NOE enhancements that exhibited the axial H-2′ with H-4′, equatorial 3′-OH, and H-6 proton of the base moiety offer further evidence of their close proximity. Finally, the lack of any essential increase in H-5′ and H-6 upon saturation of H-1′ is also in accordance with the proposed structure.

Enzyme kinetics

Calorimetric measurements (42) have shown that the binding of glucose to free GPb is accompanied by an exothermic change of −6.3 ± 0.5 kcal/mol corresponding to an average dissociation constant of 1.0 mM. Since the K_i for glucose is 1.7 mM (43), this suggests that K_i and K_d are approximately the same for glucose interactions with the enzyme. Thus, in comparative studies, differences in K_i values for closely related compounds are likely to be directly related to differences in binding energy. The inhibitory efficiency of the two compounds, GlcFU and **5,** was tested in kinetic experiments with rabbit muscle glycogen phosphorylase b (GPb) in the direction of glycogen synthesis. Both compounds displayed competitive inhibition with respect to Glc-1-P at constant concentrations of glycogen (Figure 1) and their inhibitory constants (K_i) were determined 7.9 ± 0.3 and 27.1 ± 1.4 μM, respectively. A K_i value of 5.5 ± 0.4 μM has been also recently reported (44) for GlcFU which is consistent with the one reported here, given that they have been measured in different enzyme preparations [K_m values for the substrate Glc-1-P have been reported in the range between 1 and 3 mM (45)]. Both compounds are significantly more potent than α-D-glucose (K_i = 1.7 mM) (43) possibly because of the additional interactions of the uracil group with the protein residues (10). Furthermore, they both are considerably more potent than 1-(3′-deoxy-3′-fluoro-β-D-glucopyranosyl)5-fluorouracil (Table 1, K_i = 3.67 mM) reported in our previous study (10) and other fluorodeoxy glucose derivatives which have K_i values in the mM range (46,47). This can be attributed to the presence of a hydroxyl group rather a fluoride at the 3′-equatorial position. However, the addition of a hydroxymethyl

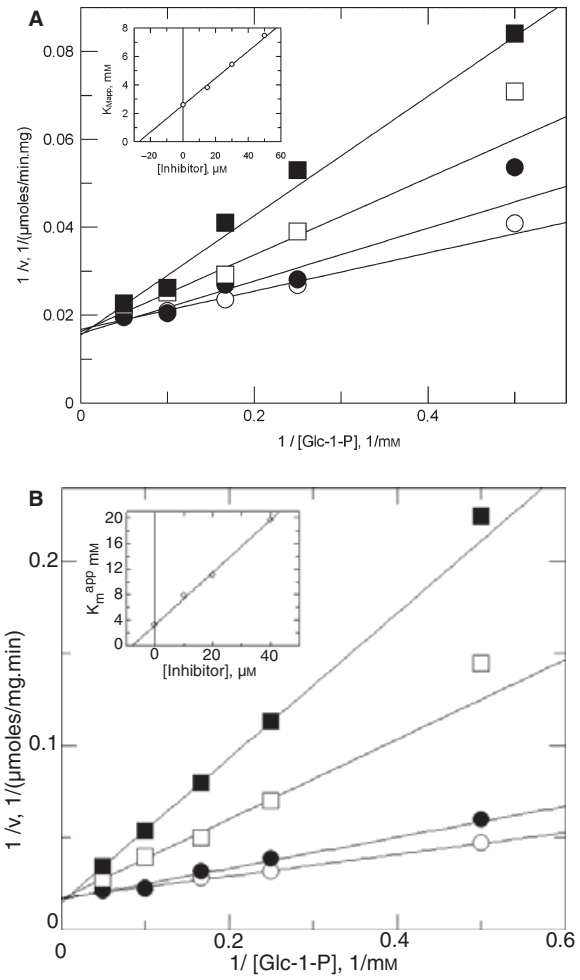

Figure 1: Lineweaver–Burk plots for the inhibition of GPb by **5** (A) and GlcFU (B) at varying concentrations of Glc-1-P. Inhibitor concentrations were as follows: 0 (○), 15 (●) 30 (□) and 50 μM (■) for compound **5** and 0 (○), 10 (●) 20 (□) and 40 μM (■) for GlcFU. Insets: Plots of Kmapp versus inhibitor concentration.

group to the glucopyranose ring at the axial position (compound **5**) did not improve the potency of GlcFU since the latter has a K_i value 3.4 times lower than **5**.

Structural studies

In order to elucidate the structural basis of inhibition and most importantly the relatively significant difference in inhibition constants, we have determined the crystal structures of GPb in complex with **5** and GlcFU. A summary of the data processing and refinement statistics for the inhibitor complex structures is given in Table 2. The 2mFo-DFc and mFo-DFc electron density maps clearly defined the position of each atom of the inhibitors (Figure 2) and specifically showed that both compounds were bound at the catalytic site. Both inhibitors bind similarly at the active site with the glucopyranose and fluorouracil moieties forming a network of hydrogen bonds and van der Walls interactions with protein residues (Figure 3, Tables S1 and S2) analogous to those observed for other glucopyranose derivatives (1) and the related 1-(3′-deoxy-3′-fluoro-β-D-glucopyranosyl)5-fluorouracil (10) in the active site of the enzyme. In addition to these interactions, the 3′-hydroxymethyl group of **5** is in hydrogen bonding distance from O2P of PLP and involved in a water-mediated interaction with O3P (Figure 3B, Table S1). Furthermore, this group is involved in polar–polar and non-polar–polar van der Waals interactions with the γ-phosphate of PLP (Table S2). Structural comparison of the parent GPb-GlcFU and GPb-**5** complexes reveals that the presence of the 3′-hydroxymethyl displaces one of the conserved water molecules (1) from the active site which mediates interactions between the γ-phosphate of PLP and the side chain of Glu672. Hence, structure activity relationship (SAR) analysis cannot account for the differences in potencies between GlcFU and **5**. On the contrary, it highlights favorable extra contacts with GPb for **5**. A more thorough energetic analysis of the ligand binding process was thus required and was realized by docking calculations followed by theoretically more thorough QM/MM-PBSA BFE calculations, where the binding contributions can be decomposed into insightful interaction and desolvation components.

Table 2: Summary of the diffraction data processing, refinement, and protein–ligand interactions statistics for GPb – inhibitor complexes

Compound	**5**	GlcFU
Resolution (Å)	13.9–2.40	13.9–2.40
Outermost shell (Å)	2.53–2.40	2.53–2.40
Reflections measured	179466	178067
Unique reflections	38290	36858
Multiplicity	4.7 (3.1)	4.8 (3.4)
R_{merge}	0.083 (0.489)	0.110 (0.497)
Completeness (%)	99.8 (98.8)	95.7 (89.4)
$\langle I/\sigma I \rangle$	14.9 (2.1)	11.5 (2.0)
R_{cryst}	0.17 (0.23)	0.18 (0.23)
R_{free}	0.22 (0.25)	0.22 (0.27)
No of solvent molecules	246	206
R.m.s. deviation from ideality		
In bond lengths (Å)	0.011	0.012
In angles (°)	1.3	1.3
Average B factor		
Protein atoms (Å^2)	27.3	23.3
Solvent molecules (Å^2)	29.9	24.3
Ligand atoms (Å^2)	17.7	12.6
Ramachandran outliers (%)	0	0
Ramachandran favored (%)	97.6	97.9
PDB code	3SYM	3SYR

Human liver GPb and rabbit muscle GPb active sites are identical in amino acid sequence and structural architecture. Structural comparison between the crystal structures of rabbit muscle GPb-**5** and human liver GPb-GlcNAc (48) complexes revealed an rmsd of 1.06 Å (all residues, all atoms) and an rmsd value for the active site residues of 0.84 Å (all atoms). Hence, it seems that there are not any differences that may impact the binding of these ligands toward their putative use as human liver GP inhibitors.

Computational results

Docking

Glide-XP docking calculations were performed to investigate the source of the greater binding affinity of GlcFU compared with **5**, results of which are shown in Table 3. Only one pose per ligand was obtained. The docking poses accurately reproduced the reported ligand crystallographic conformations, although the docking constraints dictated this to some degree. RMSDs were calculated for the ligand heavy atoms 'in-place' with just the receptors superimposed (native and docking receptor), but also for the ligands superimposed. For GlcFU, the predicted docking pose revealed 'in-place' and superimposed ligand RMSDs (heavy atoms) compared with the crystallographic conformation of 0.530 and 0.221 Å, respectively, while for **5**, the corresponding values were 0.518 and 0.268 Å, respectively.

With respect to the Glide-XP scoring, the performance of GlideScore, CvdW and Emodel scoring functions was compared. However, all three scoring function predicted **5** to be more potent than GlcFU in disagreement with our kinetics results. Numerous reasons can be given for docking failure. In the current case, it appears that given the nature of the additional interactions formed by **5** which is absent in the GlcFU complex (notably direct interactions with the γ-phosphate anion in PLP which by necessity involve some desolvation effects) that a more accurate model of solvation is necessary. QM/MM-PBSA BFE calculations exploiting the predicted docking poses were therefore performed.

QM/MM-PBSA calculations

QM/MM-PBSA calculation of binding affinities is a relatively new method based on the parent MM-GB(PB)SA approach (28) and to date has produced promising results (49–53). It has major applications in areas where standard force field-based methods may fail. For example, description of ligands using QM eliminates the problem of unparametrized or poorly parametrized ligands. Further, postprocessing of ligand poses using implicit solvation models such as PBSA and exploiting the theoretically rigorous PB method for polar (electrostatic) solvation energy contributions provides a more accurate description of solvation than the approximate methods typically used in docking (32,54).

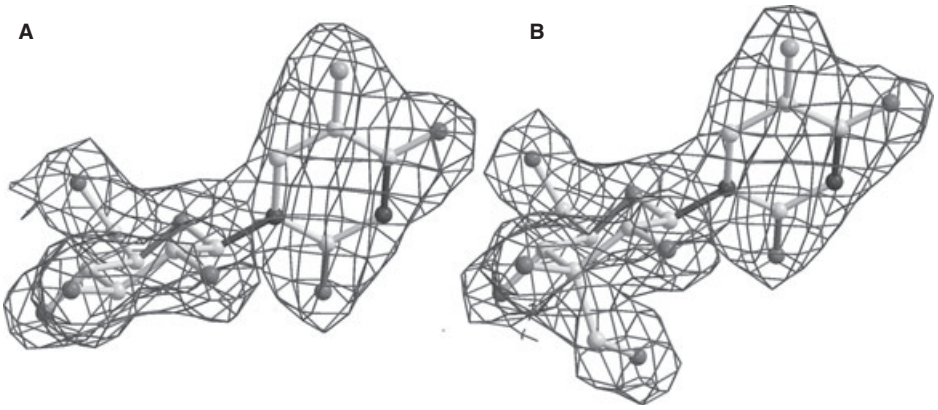

Figure 2: A Refmac 2mFo-DFc electron density maps of GlcFU (A) and **5** (B) bound at the enzyme catalytic site. The maps are contoured at 1.0σ level before the inclusion of the ligand molecule in the refinement process.

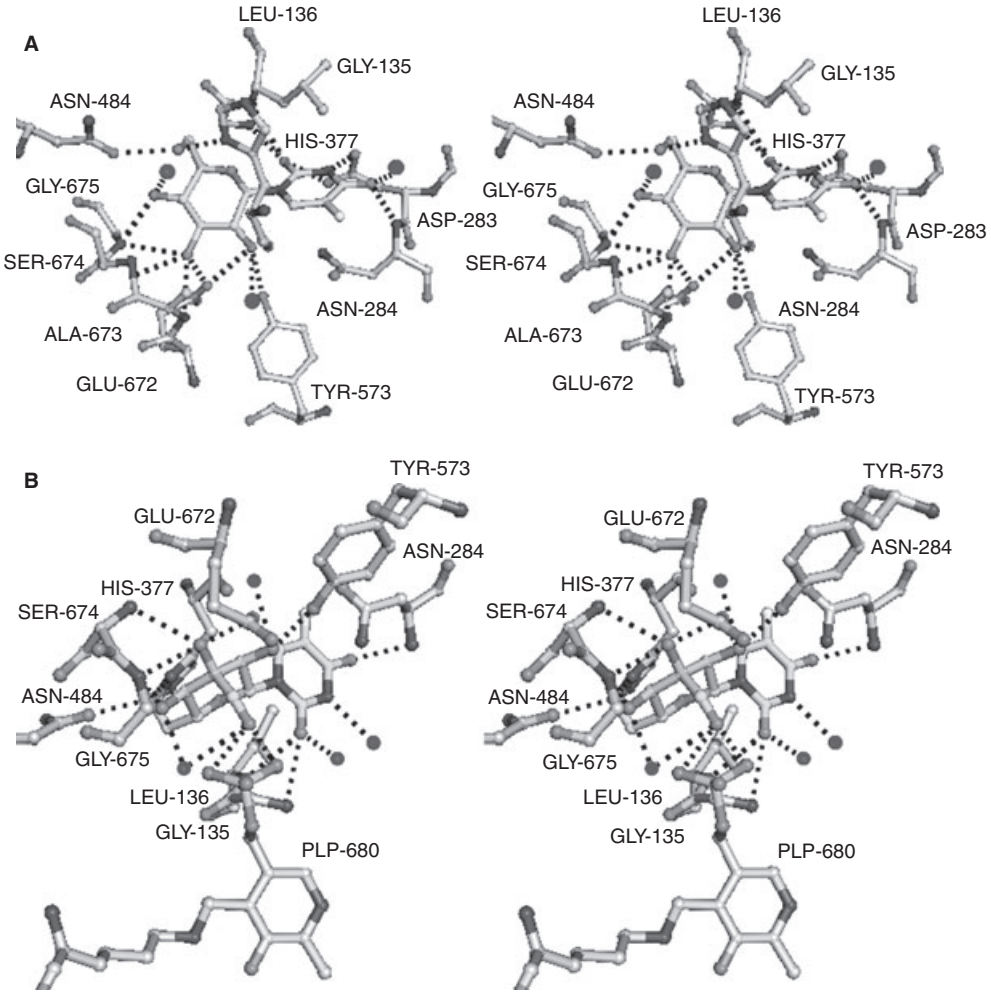

Figure 3: Stereo diagram showing the network of interactions formed between inhibitor GlcFU (A) and **5** (B) with residues at active site of GPb. Hydrogen bond interactions are represented as dotted lines and water molecules as black spheres.

The results of the QM/MM-PBSA calculations are tabulated in Table 4 where contributions to the predicted BFEs (ΔG_{bind}) are broken down into the components $\Delta E_{QM/MM}$, ΔG_{solv}, and $T\Delta S_{MM}$ from eqn 3. The ΔG_{solv} values are further decomposed into ΔG_{PB}^{solv} and ΔG_{SA}^{solv} contributions according to eqn 4. Results are given for the Glide-XP docking poses and, for comparison, the corresponding

Table 3: Results of the Glide-XP docking calculations[a]

Ligand	RMSD 'in-place' (superimposed)[b]	GS	CvdW (kcal/mol)	Emodel	Exp ΔG_{bind} (kcal/mol)[c]
GlcFU	0.530 (0.221)	−12.35	−65.1	−97.9	−7.00
5	0.518 (0.268)	−12.93	−72.1	−113.4	−6.27

[a]One docking pose was obtained for each ligand. The docking scores for the poses with three different scoring functions are compared: GlideScore (GS), a modified Coulomb – van der Waals (CvdW) interaction energy score that is formulated to avoid overly rewarding charge–charge interactions at the expense of charge–dipole and dipole–dipole interactions, and Emodel which combines GS, the interaction energy and excess internal energy of the ligand pose.
[b]RMSDs (heavy atoms) in Å 'in-place' and superimposed between the ligand docking poses and their crystallographic conformations (3SYR for GlcFU; 3SYM for **5**). The 'in-place' ligand RMSDs were calculated with receptors aligned (native and modeling receptor), but without superimposition of ligands.
[c]Values calculated using $\Delta G_{bind} = -RT\ln K_i$.

values for the 'relaxed' ligand poses (in parentheses). The relaxed geometries were obtained by QM/MM optimizations with the receptor held rigid. First of all, we note that the RMSDs (heavy atoms) between the QM/MM relaxed docking poses and their crystallographic conformations (Table 4) are mainly improved compared with the docking poses (Table 3). Next, we see that in contrast to the docking results (Table 3), GlcFU is correctly identified by the QM/MM-PBSA BFE predictions as the more potent ligand in line with our kinetics results. This outcome is observed for both the docked poses (ΔG_{bind}(GlcFU) = −70.4 kcal/mol; ΔG_{bind}(**5**) = −65.5 kcal/mol) and their QM/MM relaxed forms (ΔG_{bind}(GlcFU) = −75.8 kcal/mol; ΔG_{bind}(**5**) = −67.4 kcal/mol).

Therefore, the relative energy results from the QM/MM-PBSA calculations using both the docking poses directly and the QM/MM relaxed poses (rigid receptor) are qualitatively consistent. QM/MM-PBSA and MM-PB(GB)SA are recognized for their accuracy in prediction of relative binding affinities (51–53), which is sufficient for most applications. On the contrary, the absolute energy values are too negative, but this is also a problem with the parent MM-PB(GB)SA methodology (55) and is due to the approximations applied and inherent in these methods. Use of a rigid receptor, for example, does not account for protein relaxation and protein–ligand mutual relaxation on binding; however, a recent study revealed that better correlation between QM/MM-PBSA binding affinity predictions and experimental activities was obtained when the protein was held 'fixed' (53). This is consistent with our findings here: the QM/MM-PBSA predictions using complex geometries obtained from QM/MM optimizations including a small flexible protein region (within 4 Å of ligands) in the 'relaxation' of the docking poses did give less negative ΔG_{bind} values, but crucially incorrect ranking of ligand potencies was now obtained (Table S3).

The discussion continues with respect to the QM/MM-PBSA results for the relaxed ligand poses (receptor held rigid) from Table 4. Breakdown of the contributions to the BFEs reveals that **5** (−160.6 kcal/mol) as expected has a greater $\Delta E_{QM/MM}$ contribution to binding than GlcFU (−143.0 kcal/mol), a consequence of the extra interactions it forms and evident from our SAR analysis. However, the gains in $\Delta E_{QM/MM}$ are outweighed by the significantly larger desolvation costs for binding of **5** (ΔG_{solv} = 75.9 kcal/mol) compared with binding of GlcFU (ΔG_{solv} = 50.0 kcal/mol). Meanwhile, vibrational, rotational, and translational entropy losses ($T\Delta S_{MM}$) of the two ligands on binding are predicted to be similar (−17.2 to −17.3 kcal/mol) and do not have a notable effect on calculated relative BFEs. Loss of conformational entropy for the additional $-CH_2OH$ substituent of **5** is not accounted for in our calculations; the latter would bring the relative BFE values even more in favor of GlcFU binding (56).

Hence, (de)solvation effects are identified from our QM/MM-PBSA calculations as the source of the greater affinity for GlcFU binding. Solvation energy changes can be either enthalpy or entropy related. Analysis of the ΔG_{PB}^{solv} and the ΔG_{SA}^{solv} contributions to ΔG_{solv} for binding of each ligand reveals ΔG_{PB}^{solv} (56.2 and 82.0 for GlcFU and **5**, respectively), and therefore, solvation enthalpy changes as key to the ligand binding affinity differences. The solvation entropy change on binding is generally favorable; it is partly incorporated into the ΔG_{SA}^{solv} values and is similar for both ligands (∼−6 kcal/mol). In conclusion, for **5** to bind and interact with the PLP γ-phosphate, the solvent network around three charged residues PLP, Lys568 and Lys574 is unfavorably disrupted as judged by the ΔG_{PB}^{solv} contributions. Water molecules in a binding pocket are not equivalent and offer different binding energy contributions which are due to their local environment (57,58). The water molecules solvating charged

Table 4: Quantum Mechanics/Molecular Mechanics – Poisson–Boltzmann Surface Area (QM/MM-PBSA) results for estimation of binding free energies (BFEs)[a]

Ligand	RMSD 'in-place' (superimposed)[b]	$\Delta E_{QM/MM}$	ΔG_{PB}^{solv}	ΔG_{SA}^{solv}	ΔG_{solv}	$T\Delta S_{MM}$	ΔG_{bind}	Exp K_i (μM)
GlcFU	0.572 (0.200)	−131.9 (−143.0)	50.7 (56.2)	−6.4 (−6.2)	44.3 (50.0)	−17.2 (−17.2)	−70.4 (−75.8)	7.9
5	0.470 (0.224)	−148.3 (−160.6)	72.3 (82.0)	−6.6 (−6.1)	65.7 (75.9)	−17.1 (−17.3)	−65.5 (−67.4)	27.1

[a]Energies are in kcal/mol. Contributions to ΔG_{bind} as per eqns 3 and 4. Values are for the Glide-XP docking poses used directly in the QM/MM-PBSA calculations but with the corresponding values for the relaxed poses (preminimized using QM/MM) given in parentheses for comparison.
[b]RMSDs (heavy atoms) in Å between the QM/MM relaxed ligand docking poses and their crystallographic conformations (3SYR for GlcFU; 3SYM for **5**) 'in-place' and superimposed. The 'in-place' ligand RMSDs were calculated with receptors aligned (native and modeling receptor), but without superimposition of ligands.

species are more tightly bound and have much larger solvation free energies than neutral species. Accurate accounting (scoring) of water contributions to ligand binding is demanding (59,60). However, careful consideration of the hydration status of a protein binding pocket can lead to optimal drug design (58,60,61). The current work highlights that interference of water network surrounding anionic PLP with a 3′-axial-CH_2OH glucose substituent is not favorable; on the contrary, the gains from displacement of water molecules trapped in hydrophobic pockets are substantial (61). In this study, therefore, the benefits of a more accurate solvation model (PBSA) in accounting for the obviously significant solvation free energy changes on binding are noted, while docking results proved to be misleading.

Conclusion and Future Directions

We have successfully developed a stereoselective approach for the synthesis of novel 1-[3′-*C*-(hydroxymethyl)-β-D-glucopyranosyl]5-fluorouracil (**5**), from 3-*C*-methylene derivative **1**. The key step of this synthetic route involves the formation of pyranose nucleoside **4** during Vorbruggen sugar-base condensation reaction starting from precursor 3-*C*-acetoxymethyl-1,2,4,6-tetra-*O*-acetyl-D-glucopyranose (**3**).

Biochemical experiments have shown that **5** and GlcFU are both potent inhibitors of GPb and competitive with the substrate Glc-1-P. They are significantly better than those reported in our previous study (10). However, **5** is a weaker inhibitor than GlcFU and this cannot be explained by our SAR analysis, where additional hydrogen bond and van der Waals contacts are formed by the 3′-CH_2OH substituent of **5** with PLP. While Glide-XP docking also failed to correctly distinguish and accurately quantify the decisive binding contributions, postprocessing of the docking poses using QM/MM-PBSA binding affinity calculations correctly reflected the kinetics results. Desolvation costs for binding of **5** were determined as counter-productive to improving the binding affinity over the parent ligand GlcFU. The value of employing more accurate solvation models in postdocking methods is therefore noted (32,54), particularly when the binding interface is highly polar/charged and with the recently developed QM/MM-PBSA approach proving successful. Nevertheless, it should be finally be noted that employment of QM/MM-PBSA as a postdocking method is computationally expensive, so its application is currently limited to lead optimization studies or re-ranking of a select number of top-scoring ligands from high-throughput virtual screening (lead identification).

Acknowledgments

The authors would like to thank Prof. Georgios Archontis for useful comment during the preparation of this paper. This work was supported in part by the Postgraduate Programmes 'Biotechnology-Quality assessment in Nutrition and the Environment', 'Application of Molecular Biology-Molecular Genetics-Molecular Markers', Department of Biochemistry and Biotechnology, University of Thessaly. V.T.S., J.M.H., and S.E.Z would like to acknowledge financial support from the Commission of the European Communities – under the FP7 'SP4-Capacities Coordination and Support Action, Support Actions' EUROSTRUCT project (CSA-SA_FP7-REGPOT-2008-1 Grant Agreement No. 230146).

References

1. Somsak L., Czifrak K., Toth M., Bokor E., Chrysina E.D., Alexacou K.M., Hayes J.M., Tiraidis K., Lazoura E, Leonidas D.D., Zographos S.E., Oikonomakos N.G. (2008) New inhibitors of glycogen phosphorylase as potential antidiabetic agents. Curr Med Chem;15:2933–2983.
2. Praly J.-P., Vidal S. (2010) Inhibition of glycogen phosphorylase in the context of type 2 diabetes, with focus on recent inhibitors bound at the active site. Mini Rev Med Chem;10:1102–1126.
3. Somsak L. (2011) Glucose derived inhibitors of glycogen phosphorylase. C R Chim;14:211–223.
4. Agius L. (2010) Physiological control of liver glycogen metabolism: lessons from novel glycogen phosphorylase inhibitors. Mini Rev Med Chem;10:1175–1187.
5. Treadway J.L., Mendys P., Hoover D.J. (2001) Glycogen phosphorylase inhibitors for treatment of type 2 diabetes mellitus. Expert Opin Investig Drugs;10:439–454.
6. Agius L. (2007) New hepatic targets for glycaemic control in diabetes. Best Pract Res Clin Endocrinol Metab;21:587–605.
7. Kurukulasuriya R., Link J.T., Madar D.J., Pei Z., Richards S.J., Rohde J.J. *et al.* (2003) Potential drug targets and progress towards pharmacologic inhibition of hepatic glucose production. Curr Med Chem;10:123–153.
8. Kurukulasuriya R., Link J.T., Madar D.J., Pei Z., Rohde J.J., Richards S.J. *et al.* (2003) Prospects for pharmacologic inhibition of hepatic glucose production. Curr Med Chem;10:99–121.
9. Carpino P.A., Goodwin B. (2010) Diabetes area participation analysis: a review of companies and targets described in the 2008 – 2010 patent literature. Expert Opin Ther Pat;20:1627–1651.
10. Tsirkone V.G., Tsoukala E., Lamprakis C., Manta S., Hayes J.M., Skamnaki V.T. *et al.* (2010) 1-(3-Deoxy-3-fluoro-beta-d-glucopyranosyl) pyrimidine derivatives as inhibitors of glycogen phosphorylase b: kinetic, crystallographic and modelling studies. Bioorg Med Chem;18:3413–3425.
11. Martin J.L., Johnson L.N., Withers S.G. (1990) Comparison of the binding of glucose and glucose 1-phosphate derivatives to T-state glycogen phosphorylase b. Biochemistry;29:10745–10757.
12. Hayes J.M., Leonidas D.D. (2010) Computation as a tool for glycogen phosphorylase inhibitor design. Mini Rev Med Chem;10:1156–1174.
13. Schrodinger L.L.C. (2011) Schrodinger Software Suite. New York: Schrödinger, LLC.
14. Kim M.J. (2008) Synthesis of novel bicyclic nucleosides with 3,6-anhydro sugar moiety. Nucleosides Nucleotides Nucleic Acids;27:1097–1106.
15. Dahlman O., Garegg P.J., Mayer H., Schramek S. (1986) Synthesis of three 3-C-hydroxymethylpentoses with the D-ribo-, D-xylo- and L-lyxo-configurations. Identification of the latter with a monosaccharide isolated from phase I Coxiella burnetii lipopolysaccharide. Acta Chem Scand B;40:15–20.

16. Oikonomakos N.G., Kontou M., Zographos S.E., Watson K.A., Johnson L.N., Bichard C.J. *et al.* (1995) N-acetyl-beta-D-glucopyranosylamine: a potent T-state inhibitor of glycogen phosphorylase. A comparison with alpha-D-glucose. Protein Sci;4:2469–2477.
17. Agilent Technologies UK Ltd. (2011) CrysAlisPro Software System. Oxford, UK: Agilent Technologies UK Ltd.
18. CCP4 (1994) The CCP4 suite: programs for Protein Crystallography. Acta Crystallogr D;50:760–763.
19. Schuttelkopf A.W., van Aalten D.M.F. (2004) PRODRG: a tool for high-throughput crystallography of protein-ligand complexes. Acta Crystallogr D Biol Crystallogr;60:1355–1363.
20. Emsley P., Cowtan K. (2004) Coot: model-building tools for molecular graphics. Acta Crystallogr D Biol Crystallogr;60:2126–2132.
21. Murshudov G.N., Vagin A.A., Dodson E.J. (1997) Refinement of macromolecular structures by the Maximum-Likelihood Method. Acta Crystallogr D;53:240–255.
22. Chen V.B., Arendall W.B. III, Headd J.J., Keedy D.A., Immormino R.M., Kapral G.J. *et al.* (2010) MolProbity: all-atom structure validation for macromolecular crystallography. Acta Crystallogr D Biol Crystallogr;66:12–21.
23. Kraulis P.J. (1991) MOLSCRIPT – A program to produce both detailed & schematic plots of protein structures. J Appl Crystallogr;24:946–950.
24. DeLano W.L. (2002) The PyMol Molecular Visualization System. San Carlos, CA, USA: DeLano Scientific.
25. Dolinsky T.J., Czodrowski P., Li H., Nielsen J.E., Jensen J.H., Klebe G. *et al.* (2007) PDB2PQR: expanding and upgrading automated preparation of biomolecular structures for molecular simulations. Nucleic Acids Res;35:W522–W525.
26. Bas D.C., Rogers D.M., Jensen J.H. (2008) Very fast prediction and rationalization of pKa values for protein-ligand complexes. Proteins;73:765–783.
27. Benltifa M., Hayes J.M., Vidal S., Gueyrard D., Goekjian P.G., Praly J.-P. *et al.* (2009) Glucose-based spiro-isoxazolines: a new family of potent glycogen phosphorylase inhibitors. Bioorg Med Chem;17:7368–7380.
28. Massova I., Kollman P.A. (2000) Combined molecular mechanical and continuum solvent approach (MM-PBSA/GBSA) to predict ligand binding. Perspect Drug Dis Des;18:113–135.
29. Rastelli G., Del Rio A., Degliesposti G., Sgobba M. (2010) Fast and accurate predictions of binding free energies using MM-PBSA and MM-GBSA. J Comput Chem;31: 797–810.
30. Hayes J.M., Skamnaki V.T., Archontis G., Lamprakis C., Sarrou J., Bischler N. *et al.* (2011) Kinetics, in silico docking, molecular dynamics, and MM-GBSA binding studies on prototype indirubins, KT5720, and staurosporine as phosphorylase kinase ATP-binding site inhibitors: the role of water molecules examined. Proteins;79:703–719.
31. Kuhn B., Gerber P., Schulz-Gasch T., Stahl M. (2005) Validation and use of the MM-PBSA approach for drug discovery. J Med Chem;48:4040–4048.
32. Hou T., Wang J., Li Y., Wang W. (2011) Assessing the performance of the molecular mechanics/Poisson Boltzmann surface area and molecular mechanics/generalized Born surface area methods. II. The accuracy of ranking poses generated from docking. J Comput Chem;32:866–877.
33. Becke A.D. (1993) Density-functional thermochemistry. 3. The role of exact exchange. J Chem Phys;98:5648–5652.
34. Francl M.M., Pietro W.J., Hehre W.J., Binkley J.S., Gordon M.S., Defrees D.J. *et al.* (1982) Self-consistent molecular-orbital methods. 23. A polarization-type basis set for 2nd-row elements. J Chem Phys;77:3654–3665.
35. Murphy R.B., Philipp D.M., Friesner R.A. (2000) A mixed quantum mechanics/molecular mechanics (QM/MM) method for large-scale modeling of chemistry in protein environments. J Comput Chem;21:1442–1457.
36. Marten B., Kim K., Cortis C., Friesner R.A., Murphy R.B., Ringnalda M.N. *et al.* (1996) New model for calculation of solvation free energies: correction of self-consistent reaction field continuum dielectric theory for short-range hydrogen-bonding effects. J Phys Chem;100:11775–11788.
37. Cramer C.J., Truhlar D.G. (1999) Implicit Solvation Models: equilibria, structure, spectra, and dynamics. Chem Rev;99:2161–2200.
38. Israelachvili J.N. (2011) Intermolecular and Surface Forces. Boston, MA: Academic Press.
39. Haeckel R., Weber K., Germann C., Haberkorn U., Zeisler S., Eisenbarth J. *et al.* (1996) Synthesis of F-18 labelled nucleoside analogues. J Labelled Comp Radiopharm;38:1061–1070.
40. Acton E.M., Goerner R.N., Uh H.S., Ryan K.J., Henry D.W., Cass C.E. *et al.* (1979) Improved antitumor effects in 3′-branched homologues of 2′-deoxythioguanosine. Synthesis and evaluation of thioguanine nucleosides of 2,3-dideoxy-3-(hydroxymethyl)-D-erythro-pentofuranose. J Med Chem;22:518–525.
41. Vorbruggen H., Hofle G. (1981) Nucleoside syntheses. 23. On the mechanism of nucleoside synthesis. Chemische Berichte-Recueil;114:1256–1268.
42. Steiner R.F., Greer L., Bhat R., Oton J. (1980) Structural changes induced in glycogen phosphorylase b by the binding of glucose and caffeine. Biochim Biophys Acta;611:269–279.
43. Martin J.L., Veluraja K., Ross K., Johnson L.N., Fleet G.W.J., Ramsden N.G. *et al.* (1991) Glucose analogue inhibitors of glycogen phosphorylase: the design of potential drugs for diabetes. Biochemistry (USA);30:10101–10116.
44. Gimisis T. (2010) Synthesis of N-glucopyranosidic derivatives as potential inhibitors that bind at the catalytic site of glycogen phosphorylase. Mini Rev Med Chem;10:1127–1138.
45. Oikonomakos N.G. (2002) Glycogen phosphorylase as a molecular target for type 2 diabetes therapy. Curr Protein Pept Sci;3:561–586.
46. Street I.P., Armstrong C.R., Withers S.G. (1986) Hydrogen bonding and specificity. Fluorodeoxy sugars as probes of hydrogen bonding in the glycogen phosphorylase-glucose complex. Biochemistry;25:6021–6027.
47. Sprang S.R., Goldsmith E.J., Fletterick R.J., Withers S.G., Madsen N.B. (1982) Catalytic site of glycogen phosphorylase: structure of the T state and specificity for alpha-D-glucose. Biochemistry;21:5364–5371.
48. Rath V.L., Ammirati M., LeMotte P.K., Fennell K.F., Mansour M.N., Danley D.E. *et al.* (2000) Activation of human liver glycogen phosphorylase by alteration of the secondary structure and packing of the catalytic core. Mol Cell;6:139–148.
49. Retegan M., Milet A., Jamet H. (2009) Exploring the binding of inhibitors derived from tetrabromobenzimidazole to the CK2

protein using a QM/MM-PB/SA approach. J Chem Inf Model;49:963–971.
50. Soderhjelm P., Kongsted J., Ryde U. (2010) Ligand affinities estimated by quantum chemical calculations. J Chem Theor Comput;6:1726–1737.
51. Wang M., Wong C.F. (2007) Rank-ordering protein-ligand binding affinity by a quantum mechanics/molecular mechanics/Poisson–Boltzmann-surface area model. J Chem Phys;126:026101.
52. Grater F., Schwarzl S.M., Dejaegere A., Fischer S., Smith J.C. (2005) Protein/ligand binding free energies calculated with quantum mechanics/molecular mechanics. J Phys Chem B;109: 10474–10483.
53. Ciancetta A., Genheden S. (2011) A QM/MM study of the binding of RAPTA ligands to cathepsin B. J Comput Aided Mol Des;25:729–742.
54. Lindstrom A., Edvinsson L., Johansson A., Andersson C.D., Andersson I.E., Raubacher F. *et al.* (2011) Postprocessing of docked protein–ligand complexes using implicit solvation models. J Chem Inf Model;51:267–282.
55. Singh N., Warshel A. (2010) Absolute binding free energy calculations: on the accuracy of computational scoring of protein-ligand interactions. Proteins;78:1705–1723.
56. Lazaridis T., Masunov A., Gandolfo F. (2002) Contributions to the binding free energy of ligands to avidin and streptavidin. Proteins;47:194–208.
57. Jia R., Yang L.-J., Yang S.-Y. (2008) Binding energy contributions of the conserved bridging water molecules in CDK2-inhibitor complexes: a combined QM/MM study. Chem Phys Lett;460: 300–305.
58. Barillari C., Taylor J., Viner R., Essex J.W. (2007) Classification of water molecules in protein binding sites. J Am Chem Soc; 129:2577–2587.
59. Li Y., Sutch B.T., Bui H.H., Gallaher T.K., Haworth I.S. (2011) Modeling of the water network at protein-RNA interfaces. J Chem Inf Model;51:1347–1352.
60. de Beer S.B., Vermeulen N.P., Oostenbrink C. (2010) The role of water molecules in computational drug design. Curr Top Med Chem;10:55–66.
61. Homans S.W. (2007) Water, water everywhere – except where it matters? Drug Discov Today;12:534–539.

Supporting Information

Additional Supporting Information may be found in the online version of this article:

Figure S1. NOE measurements performed on compound **4**.

Table S1. Hydrogen bond interactions of the inhibitors with residues at the catalytic site of GPb in the crystal.

Table S2. Potential van der Waals interactions of compounds GlcFU and **5** with GPb residues upon binding to the catalytic site.

Table S3. QM/MM-PBSA results for estimation of binding free energies (BFEs) using ligand docking poses 'relaxed' including a small flexible protein region[a]

Please note: Wiley-Blackwell is not responsible for the content or functionality of any supporting materials supplied by the authors. Any queries (other than missing material) should be directed to the corresponding author for the article.